Journal of Medicinal Chemistry

pubs.acs.org/jmc

Article

Expanding Structure–Activity Relationships of Human Urotensin II Peptide Analogues: A Proposed Key Role of the N-Terminal Region for Novel Urotensin II Receptor Modulators

Francesco Merlino,* Agnese Secondo, Emma Mitidieri, Raffaella Sorrentino, Rosa Bellavita, Nicola Grasso, David Chatenet, Anna Pannaccione, Paolo Grieco,* Roberta d'Emmanuele di Villa Bianca,⊥ and Alfonso Carotenuto⊥

Cite This: J. Med. Chem. 2024, 67, 13879–13890

Read Online

ACCESS | Metrics & More | Article Recommendations | Supporting Information

ABSTRACT: While the urotensinergic system plays a role in influencing various pathologies, its potential remains untapped because of the absence of therapeutically effective urotensin II receptor (UTR) modulators. Herein, we developed analogues of human urotensin II (*h*U-II) peptide in which, along with well-known antagonist-oriented modifications, the Glu[1] residue was subjected to single-point mutations. The generated library was tested by a calcium mobilization assay and ex vivo experiments, also in competition with selected ligands. Interestingly, many derivatives showed noncompetitive modulation that was rationalized by the lateral allostery concept applied to a G protein-coupled receptor (GPCR) multimeric model. **UPG-108** showed an unprecedented ability to double the efficacy of *h*U-II, while **UPG-109** and **UPG-111** turned out to be negative allosteric modulators of UTR. Overall, our investigation will serve to explore and highlight the expanding possibilities of modulating the UTR system through N-terminally modified *h*U-II analogues and, furthermore, will aim to elucidate the intricate nature of such a GPCR system.

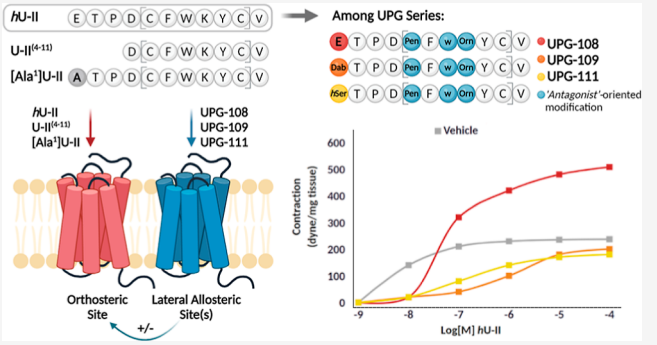

INTRODUCTION

The urotensinergic system, which is involved in the physiological regulation of many mammalian organ systems, is composed of a G protein-coupled receptor (GPCR) [urotensin II receptor (UTR)] and two endogenous peptide ligands, urotensin II (U-II) and urotensin II-related peptide (URP).[1−3] U-II is a cyclic peptide consisting of the human isoform of 11 amino acids ETPD[CFWKYC]V (*h*U-II) (**1**, Chart 1), where the cyclic structure is due to a disulfide bond between the two cysteine residues.[2,4,5] URP, a paralog of *h*U-II, of sequence A[CFWKYC]V, shares structural similarities with *h*U-II as it contains the characteristic cyclic bioactive core.[6,7] Both of these ligands can interact with UTR stabilizing different conformations of it.[1,8,9] Accordingly, these ligands have the potential to trigger distinct signaling patterns and functional outcomes, which could contribute differently to the development of diseases affected by the dysregulation of the urotensinergic system.[10] This system is crucial to regulate cardiovascular homeostasis, and U-II has been recognized among the most potent natural vasoconstrictive peptides.[11,12] During the last decades, this system has also been associated with the modulation and progression of different pathological conditions,[1,13,14] including pulmonary arterial hypertension,[15] atherosclerosis,[16] heart failure,[17] asthma,[18] inflammatory responses,[19−21] diabetes,[22] erectile dysfunction,[23,24] renal failure,[25] and cancer.[26−28] Gaining a deeper understanding of the molecular factors involved in the interaction between *h*U-II and **URP** and the UTR, as well as the molecular and cellular pharmacology of this system, is essential for advancing the development of new ligands with clinical potential.

Among the most significant derivatizations of these ligands, the Ala-scan of *h*U-II contributed to the discovery of one derivative, [**Ala**[1]]**U-II**, ATPD[CFWKYC]V (**2**, Chart 1), which was endowed with both affinity and activity toward human UTR comparable to the native *h*U-II.[29] In the same study, which was later supported by another work,[30] it was demonstrated that replacement of any endocyclic by an alanine or its D-isomer or even their deletion resulted in marginal or no loss of binding, which was linked to the bioactive cyclic core

Received: March 25, 2024
Revised: July 2, 2024
Accepted: July 25, 2024
Published: August 3, 2024

Chart 1. Structures of Selected Reference UTR Ligands Used in This Study: *h*U-II (1), [Ala^1]U-II (2), U-II$^{(4-11)}$ (3), and urantide (4). "Agonist" and "Antagonist" Cyclic Sequences are Highlighted in Dark Blue and Dark Red, Respectively

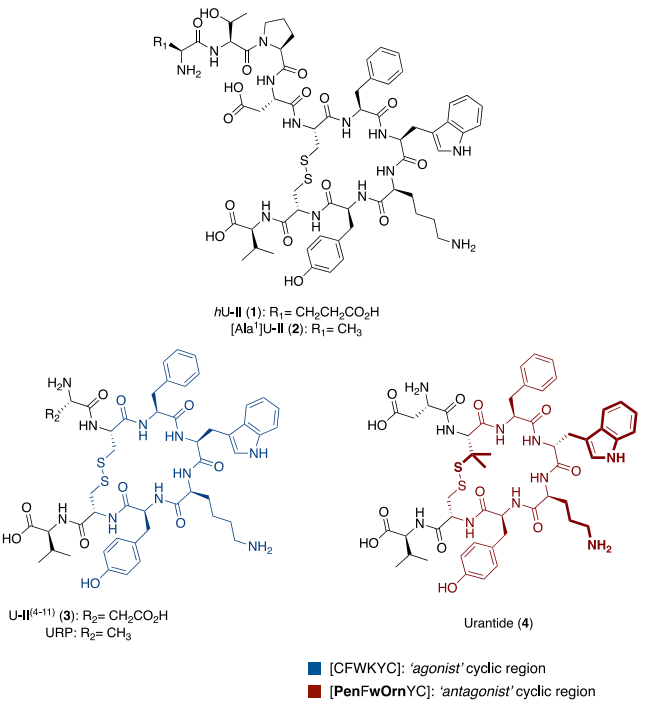

[CFWKYC]. Additional exocyclic and endocyclic modifications contributed to revealing that the sequential deletion of exocyclic residues from the N-terminal of the *h*U-II sequence was not detrimental to the calcium-mobilizing effects, while removal of any residue within the cyclic region reduced or abolished the biological activity. Therefore, the shortest, fully potent sequence of *h*U-II, the octapeptide U-II$^{(4-11)}$, D-[CFWKYC]V (**3**, Chart 1), was identified as the minimal active sequence and used for subsequent hit-to-lead optimizations.[29−32] In particular, **urantide**, developed through specific amino acid replacements (D[**PenFwOrn**YC]V, **4**, Chart 1), was identified as an antagonist.[33]

UTR antagonists could serve as valuable therapeutic agents for treating multiple pathologies.[15−18,34−37] Unfortunately, preliminary clinical investigations of UTR antagonist candidates have demonstrated limited effectiveness in humans.[1] Previously developed peptide and nonpeptide antagonists, such as urantide and palosuran, respectively, have failed to show efficacy in various preclinical models.[15,16,34−37] However, extensive studies on structure−activity relationships (SARs) upon *h*U-II and URP sequences have allowed the generation of different agonists and antagonists by enhancing our understanding of the structural requirements for interacting with the UTR.[31,32,38−41] The absence of specific and effective antagonists still hampers therapeutic intervention targeting this system. Moreover, most recent discoveries related to the biased agonism of *h*U-II and URP versus UTR could call into question some structural modifications previously applied and long consolidated to finally determine a repositioning of the SAR information in our hands.

In this work, we aimed to provide new ***h*U-II** and **urantide** analogues restored by the N-terminal tripeptide tail to determine its contribution to the development of finer and more useful UTR ligands. The generated compounds were tested by a calcium mobilization assay in HEK-293 cells stably expressing human UTR and ex vivo experiments in rat aorta, also in competition with cumulative concentration response of known ligands, raising their potential in the modulation of the UTR system and finally providing valuable information to the pre-existing SAR knowledge.

RESULTS

Design. A focused library of U-II analogues was designed starting from *h*U-II and urantide sequences (Table 1). First, to evaluate the contribution of the N-terminal residues, i.e., Glu^1-Thr^2-Pro^3, the "antagonist" cyclic region of urantide, [Pen-Phe-DTrp-Orn-Tyr-Cys], was inserted into the *h*U-II sequence (analogue **UPG-106**). Then, the Glu^1 residue was subjected to single-point modifications by substitutions with different residues of neutral or positively charged side chains but similar steric hindrance to achieve analogues **UPG-107−109** and **UPG-111**. In one additional derivative, **UPG-112**, negatively charged residues, Glu^1 and Asp^4, of the ***h*U-II** *N*-terminus were both replaced with an alanine residue. Finally, based on results obtained by calcium mobilization assays related to **UPG-109** and **UPG-111**, 2,4-diaminobutyric acid (Dab) and homoserine (*h*Ser) amino acids were also used to replace the first residue (Glu^1) within the sequence of ***h*U-II** itself, thus carrying the "agonist" cyclic region, and so obtaining derivatives **UPG-110** and **UPG-113**, respectively.

Table 1. Reference UTR Peptide Ligands Used in This Study and Novel *h*U-II (1)/Urantide (4) Derivative Sequences

ID	sequence[a]
reference UTR peptide ligands	
*h*U-II (**1**)	ETPD[CFWKYC]V
[Ala^1]U-II (**2**)	**A**TPD[CFWKYC]V
U-II$^{(4-11)}$ (**3**)	D[CFWKYC]V
urantide (**4**)	D[**PenFwOrn**YC]V
novel *h*U-II/urantide derivatives	
UPG106	ETPD[**PenFwOrn**YC]V
UPG107	**A**TPD[**PenFwOrn**YC]V
UPG108	**Q**TPD[**PenFwOrn**YC]V
UPG109	**Dab**TPD[**PenFwOrn**YC]V
UPG111	***h*Ser**TPD[**PenFwOrn**YC]V
UPG112	**A**TP**A**[**PenFwOrn**YC]V
UPG110	**Dab**TPD[CFWKYC]V
UPG113	***h*Ser**TPD[CFWKYC]V

[a]Amino acids in replacement of those originally belonging to the native ***h*U-II** sequence are bolded.

Synthesis. Linear precursors of peptides **UPG-106−113** were assembled by following the Fmoc-based solid-phase peptide synthesis assisted by ultrasonication (US-SPPS).[42] This methodology was employed to carry out Fmoc deprotection [20% piperidine in dimethylformamide (DMF), 0.5 + 1 min] and coupling [(1-cyano-2-ethoxy-2-oxoethylidenaminooxy)dimethylamino-morpholino-carbenium hexafluorophosphate (COMU)/ethyl cyano(hydroxyimino)-acetate (Oxyma Pure) as activating/additive agents, ultrasonic irradiation, 5 min treatment], which were cyclically performed until the accomplishment of the resin-bound target linear peptide sequences. Upon treatment with a solution of

https://doi.org/10.1021/acs.jmedchem.4c00688
J. Med. Chem. 2024, 67, 13879−13890

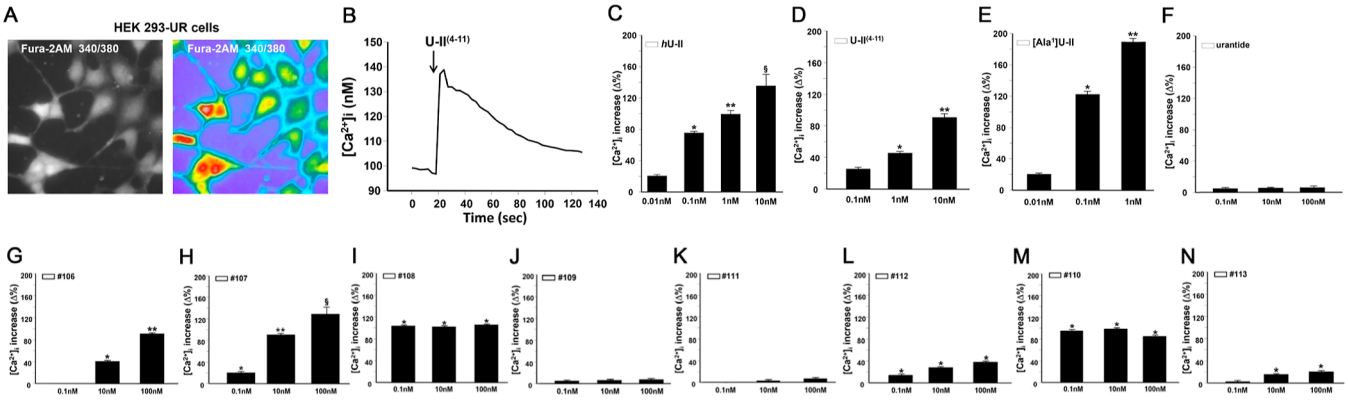

Figure 1. Effect of UTR peptide ligands and derivatives on $[Ca^{2+}]_i$ increase in HEK-293 transfected with the human form of UTR. (A) Representative fluorescent images of HEK-293 stably expressing the human form of UTR (HEK-293-UR cells) and loaded with Fura-2 AM. (B) Representative trace for the effect of **U-II**$^{(4-11)}$ on intracellular calcium concentration, $[Ca^{2+}]_i$, increase in HEK-293-UR measured on single cells. (C−F) Concentration-dependent curves for the effect of *h***U-II** (C), **U-II**$^{(4-11)}$ (D), [**Ala**^{1}]**U-II** (E), and **urantide** (F) on $[Ca^{2+}]_i$. Each concentration has been tested on at least 15 cells in HEK-293-UR culture loaded with Fura-2AM. $^*p < 0.05$ vs basal values of $[Ca^{2+}]_i$ and previous concentration, $^{**}p < 0.05$ vs previous concentrations, $^{\S}p < 0.05$ vs all. (G−N) Concentration-dependent curves (0.1−100 nM) for the effect of derivatives **UPG-106** (G), **UPG-107** (H), **UPG-108** (I), **UPG-109** (J), **UPG-111** (K), **UPG-112** (L), **UPG-110** (M), and **UPG-113** (N) on $[Ca^{2+}]_i$. Each concentration has been tested on at least 12 cells in HEK-293-UR culture loaded with Fura-2AM. $^*p < 0.05$ vs basal values of $[Ca^{2+}]_i$ and previous concentration, $^{**}p < 0.05$ vs previous concentrations, and $^{\S}p < 0.05$ vs all.

trifluoroacetic acid (TFA), peptides were cleaved from the resin as linear sequences. The cyclization between cysteines to achieve disulfide bridges was obtained by dissolving the crude peptide in water to a final peptide concentration of 0.5 mM and then adding an aqueous solution of *N*-chlorosuccinimide (NCS).[43] After cleavage, crude peptides **UPG-106−113** were purified by reversed-phase high-pressure liquid chromatography (RP-HPLC) and characterized by high-resolution mass spectrometry (HRMS) with agreement between calculated and experimentally found molecular weights (see the Supporting Information).

Calcium Mobilization Assay on Single Cells. UTR being a G_q protein-coupled receptor, peptides were preliminarily assessed in vitro by a calcium mobilization assay (Figure 1). The intracellular calcium concentration, $[Ca^{2+}]_i$, was monitored in HEK-293 cells stably expressing the human form of UTR. *h***U-II**, **U-II**$^{(4-11)}$, and [**Ala**^{1}]**U-II**, taken as reference compounds, elicited a significant increase in $[Ca^{2+}]_i$. In particular, the administration of both *h***U-II** (0.01−10 nM) and **U-II**$^{(4-11)}$ (0.1−10 nM) resulted in a rapid and concentration-dependent $[Ca^{2+}]_i$ increase with EC_{50}'s of 0.6 ± 0.002 nM and 1.2 ± 0.003 nM, respectively. Interestingly, [**Ala**^{1}]**U-II** elicited a more pronounced $[Ca^{2+}]_i$ increase in the range of concentrations of 0.01−1 nM, displaying the highest potency and efficacy. On the other hand, the UT antagonist **urantide** (0.1−100 nM) only produced a very low $[Ca^{2+}]_i$ increase in HEK-293 transfected cells.

The novel *h***U-II**/**urantide** derivatives were investigated by a calcium mobilization assay. Among peptides **UPG-106−109**, **UPG-111**, and **UPG-112** (Figure 1G−L), all including the "antagonist" cyclic core, derivatives **UPG-109** and **UPG-111** behaved similarly to **urantide** (Figure 1J,K), while, in contrast, peptides **UPG-106**, **UPG-107**, and **UPG-108** were able to highly increase $[Ca^{2+}]_i$ in the order **UPG-106** < **UPG-107** < **UPG-108** (Figure 1G−I). These outcomes suggested that the first residue of the N-terminal tail can influence the ability to mobilize intracellular calcium, regardless of the "antagonistic" cyclic core placed in C-terminus. Noteworthy, **UPG-108**, bearing Gln^1, was able to fully activate the receptor already at the lowest concentration tested, i.e., 0.1 nM, and produce a similar effect at the highest concentrations. Moreover, **UPG-107**, with the Ala^1 mutation, showed activity very similar to that of the agonists *h***U-II** and **U-II**$^{(4-11)}$. The analogue **UPG-112**, in which both negatively charged residues of the tail Glu^1 and Asp^4 were replaced by Ala, resulted in a less effective $[Ca^{2+}]_i$ mobilization compared to **UPG-107**, pointing out that the presence of a negative charge in this region of the sequence is needed for more antagonist-oriented effects (Figure 1L). Based on these results, the two amino acids leading to less active analogues, i.e., Dab (**UPG-109**) and *h*Ser (**UPG-111**), were selected and placed in the full agonist sequence of the *h***U-II**, thus testing compounds **UPG-110** and **UPG-113**. Hence, Glu to Dab replacement in compound **UPG-110** did not show the same impact (vs **UPG-109**) as it was able to highly increase $[Ca^{2+}]_i$ even at 0.1 nM (Figure 1M). However, **UPG-113** showed low potency and efficacy, confirming that Glu to *h*Ser substitution, despite the presence of the "agonist" cyclic sequence, still negatively impacted the activation of receptor-mediated calcium signaling, as for **UPG-111** (Figure 1N).

Rat Aorta Ring Contraction Assay. All derivatives (peptides **UPG-106−113**) were then investigated for their ability to induce rat aortic ring contraction. Hence, analogues containing the intracyclic sequence of **urantide** (peptides **UPG-106−109**, **UPG-111**, and **UPG-112**) were devoid of contractile activity, while only peptides keeping the "agonist" cyclic region, such as **UPG-110** and **UPG-113**, were able to stimulate ring contraction (Figure 2). Similarly to *h***U-II**, these compounds showed a concentration−response curve and reached a plateau in the range of 0.3−1 μM. More specifically, the contracting effect of **UPG-113** was significantly higher compared to **UPG-110**, consisting of a significant increase in efficacy (E_{max} 97.78 ± 4.2 dyn/mg tissue for **UPG-110** vs E_{max} 144.2 ± 9.3 dyn/mg tissue for **UPG-113**, $^{**}p < 0.01$) but not in potency. The efficacy of both peptides was significantly lower than that of *h***U-II** (E_{max} 237.2 ± 9 dyn/mg tissue; $^{°°°}p < 0.001$), making these peptides partial agonists.

https://doi.org/10.1021/acs.jmedchem.4c00688
J. Med. Chem. 2024, 67, 13879−13890

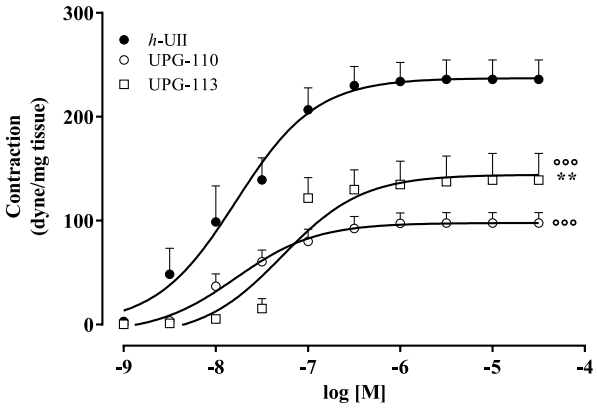

Figure 2. Effect of **UPG-110** and **UPG-113** in rat aortic rings deprived of the endothelium. **UPG-110** (1 nM−30 μM) or **UPG-113** (1 nM−30 μM) contracted aortic rings in a concentration-dependent manner. The contracting response (E_{max}) of **UPG-110** and **UPG-113** was lower than *h***U-II** (°°°$p < 0.001$). The concentration induced by **UPG-113** showed a higher efficacy (E_{max}) compared to **UPG-110** (**$p < 0.01$). Values shown are means ± SEM ($n = 5$) and are expressed as dyne/mg tissue.

Rat Aorta Ring Contraction Competition Assay. Peptides unable to induce rat aortic ring contraction (**UPG-106−109**, **UPG-111,** and **UPG-112**) were assessed for their ability to prevent a cumulative concentration−response curve of *h***U-II**, **U-II**$^{(4-11)}$, and [**Ala**^{1}]**U-II** (1 nM−30 μM) (Figure 3, Tables 2 and S2).

Following these conditions, peptide **UPG-106** acted as an antagonist when tested with *h***U-II**, as it significantly reduced *h***-UII**-induced contraction in terms of potency at all concentrations tested (Figure 3A and Table S2). However, peptide **UPG-106** significantly increased the *h***U-II** efficacy at 1 μM and significantly reduced the *h***U-II** efficacy at 10 μM (Table 2). Against **U-II**$^{(4-11)}$, at the lowest tested concentration, **UPG-106** significantly increased its efficacy, with a weak decrease in potency (Figure 3B and Table S2); at 1 μM concentration, **UPG-106** changed neither the efficacy nor the potency of **U-II**$^{(4-11)}$, while at 10 μM concentration, it strikingly reduced the potency (Figure 3B, Tables 2 and S2). **UPG-106** at 0.1 and 10 μM decreased both efficacy and potency of [**Ala**^{1}]**U-II**-induced contraction, while at an intermediate concentration such as 1 μM, it did not affect the [**Ala**^{1}]**U-II** response (Figure 3C and Table S2).

Peptide **UPG-107**, which can be considered an analogue of [**Ala**^{1}]**U-II** bearing the "antagonist" cyclic region, acted as an antagonist as it significantly reduced the *h***U-II** potency at all concentrations tested (Figure 3D and Table S2). As for the efficacy, only the intermediate concentration increased the efficacy of *h***U-II** (Table 2). Intriguingly, at both 0.1 and 1 μM concentrations, a significant enhancement of the efficacy of **U-II**$^{(4-11)}$ was observed. Moreover, peptide **UPG-107** reduced the potency of **U-II**$^{(4-11)}$ at concentrations of 0.1 and 10 μM (Figure 3E and Table S2). Peptide **UPG-107** was able to significantly reduce the potency of [**Ala**^{1}]**U-II** at higher concentrations (Figure 3F and Table S2) and the efficacy at the lowest and highest concentrations (Table 2).

Regarding peptide **UPG-108**, it collectively showed a significant concentration-dependent reduction in the potency of *h***U-II** (Figure 3G and Table S2), acting as an antagonist. This reduction in potency is combined with an increase in efficacy at lower concentrations (Table 2). A similar profile was found versus **U-II**$^{(4-11)}$ in terms of potency (Figure 3H and Table S2) and efficacy (Table 2). Interestingly, peptide **UPG-108** significantly reduced the potency of [**Ala**^{1}]**U-II** at 1 and 10 μM (Figure 3I and Table S2), while its efficacy was significantly increased at the intermediate concentration and reduced at the highest concentration (10 μM) (Table 2).

Peptide **UPG-109** exhibited a concentration-dependent reduction in potency against all three agonist probes. At all concentrations tested, peptide **UPG-109** significantly reduced the potency of *h***U-II** (Figure 3J and Table S2), **U-II**$^{(4-11)}$ (Figure 3K and Table S2), and [**Ala**^{1}]**U-II** (Figure 3L and Table S2). Furthermore, at the 1 μM concentration, peptide **UPG-109** improved the efficacy of *h***U-II**, while at the concentrations of 0.1 and 10 μM, it decreased the efficacy of *h***U-II**, although not significantly (Table 2). Regarding **U-II**$^{(4-11)}$, peptide **UPG-109** at 0.1 and 10 μM significantly reduced efficacy (Table 2). Against [**Ala**^{1}]**U-II**, peptide **UPG-109** showed a significant reduction in the efficacy at all concentrations tested (insurmountable antagonist) (Table 2).

Peptide **UPG-111** showed a concentration-dependent reduction in potency against all three agonist probes. At all concentrations tested, it significantly reduced the potency of *h***U-II** (Figure 3M and Table S2), **U-II**$^{(4-11)}$ (Figure 3N and Table S2), and [**Ala**^{1}]**U-II** (Figure 3O and Table S2). Interestingly, peptide **UPG-111** weakly reduced the efficacy of *h***U-II**, showing a significant effect only at 1 μM (Table 2). Furthermore, all concentrations of peptide **UPG-111** significantly decreased the efficacy of **U-II**$^{(4-11)}$, while only the lowest concentration (0.1 μM) increased the efficacy of [**Ala**^{1}]**U-II** (Table 2).

Peptide **UPG-112** did not affect the potency of all three agonist probes (Figure 3P−R). It showed a noncanonical profile in terms of efficacy against *h***U-II**, showing an increase at the intermediate concentration and a decrease at 10 μM (Table 2). Interestingly, peptide **UPG-112** at 0.1 and 1 μM increased the **U-II**$^{(4-11)}$ efficacy with no effect at the highest concentration (Table 2). Finally, peptide **UPG-112** exclusively at the lowest concentration of 0.1 μM significantly increased the [**Ala**^{1}]**U-II** effect resulting in greater efficacy (Table 2).

DISCUSSION AND CONCLUSIONS

Most research on urotensin analogues has focused on the design of orthosteric antagonists, while little has been done toward the discovery of various allosteric modulators of the UTR, which could open new opportunities for the development of more effective molecules acting on the urotensinergic system and limit side effects of the nonselective engagement by other ligands.

Taking into account modifications on the N-terminus of *h***U-II**, it has been long considered that this region, outside the cyclic core, is not essential for functionality, and its truncated derivatives, such as **U-II**$^{(4-11)}$ sequence, are known to retain both binding affinity and intracellular calcium mobilization, resulting in a vasocontractile action comparable with the native ligand.[29] However, more recent findings suggested that this region may have specific interactions with the UTR, causing important topological changes in the UTR conformation and therefore changes in the activation of the receptor itself.[1,8,38,44] This led us to explore novel modifications of *h***U-II** and **urantide**, along with key single-point modifications occurring in the N-terminal residues, with the further aim of obtaining novel peptides of potential modulatory effects on the UTR. Our designed library was assessed in vitro for intracellular

https://doi.org/10.1021/acs.jmedchem.4c00688
J. Med. Chem. 2024, 67, 13879−13890

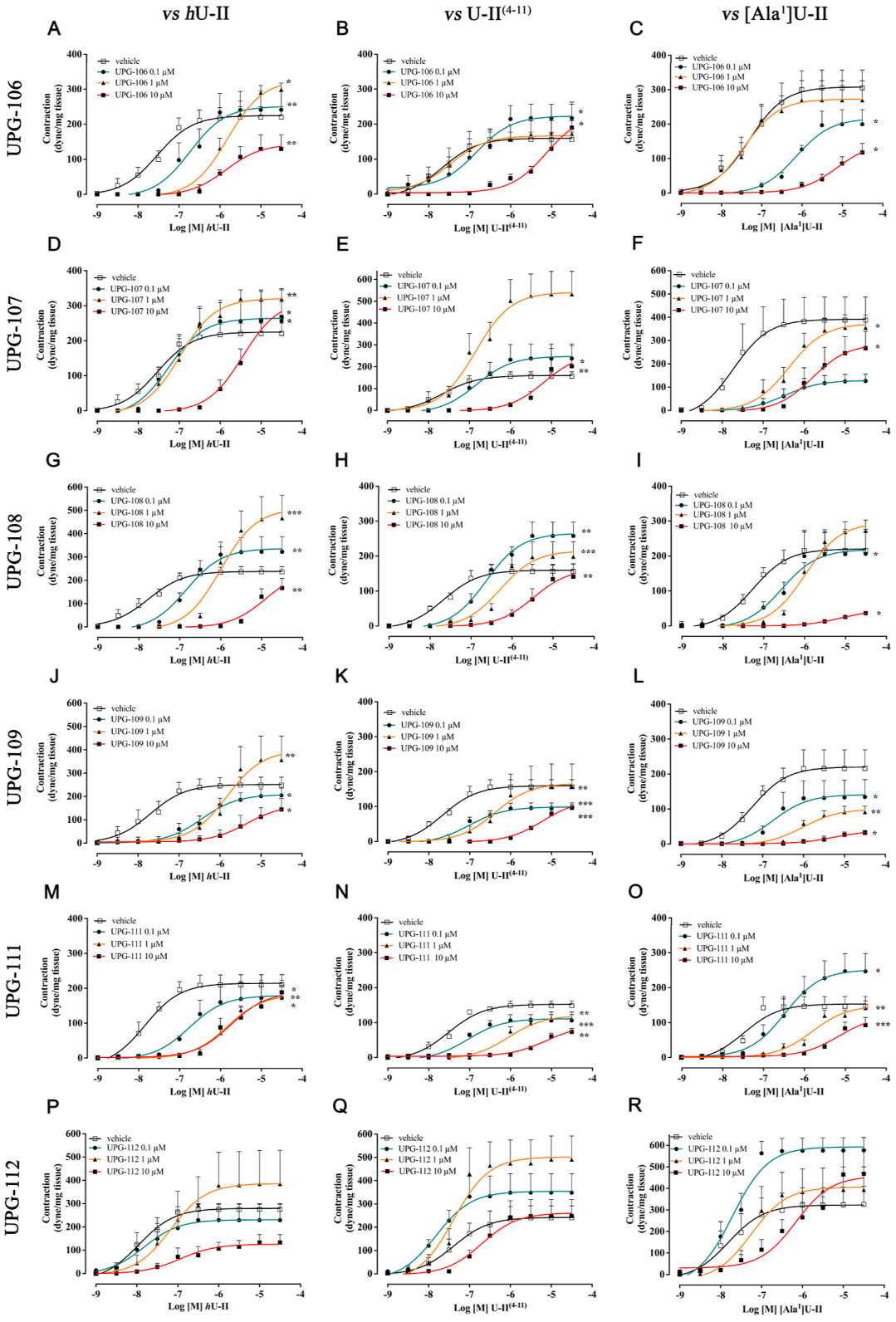

Figure 3. Effect of peptides **UPG-106** (A−C), **UPG-107** (D−F), **UPG-108** (G−I), **UPG-109** (J−L), **UPG-111** (M−O), and **UPG-112** (P−R) on *h***U-II**-, **U-II**$^{(4-11)}$-, and [**Ala**^{1}]**U-II**-induced contraction in rat aorta rings deprived of the endothelium. The aortic tissues were incubated with three different UPG peptide concentrations (0.1 μM, teal blue; 1 μM, orange; and 10 μM, red), or vehicle (black), and then stimulated with *h***U-II**, **U-II**$^{(4-11)}$, and [**Ala**^{1}]**U-II** (1 nM−30 μM). The values shown are reported as mean ± SEM (n = 5), and the concentration−response curves are expressed as dyne/mg tissue. The statistical analysis is referred to EC_{50} values (*p < 0.05; **p < 0.001; ***p < 0.001 vs own vehicle).

calcium release in HEK-293 cells transfected with human UTR and ex vivo for vasoconstriction activity on rat aortic rings. Considering that UTR in primates and rodents exhibits substantially different pharmacological profiles due to a variance in the kinetics of ligand−receptor dissociation attributed to species specificity,[45,46] and being aware of this

https://doi.org/10.1021/acs.jmedchem.4c00688
J. Med. Chem. 2024, 67, 13879−13890

Table 2. E_{max} Values for UTR Ligands against UPG-106-109, UPG-111, and UPG-112

	E_{max}[a]											
	vs *h*U-II				vs U-II$^{(4-11)}$				vs [Ala^1]U-II			
	vehicle	0.1 μM	1 μM	10 μM	vehicle	0.1 μM	1 μM	10 μM	vehicle	0.1 μM	1 μM	10 μM
UPG-106	224.8 ± 11.71	251.6 ± 22.83	327 ± 16.88***	143.5 ± 17.84**	159.8 ± 7.39	223.4 ± 20.65*	166.6 ± 17.39	231 ± 53.76*	308.1 ± 21.4	216.19 ± 17.34**	727.7 ± 20.17	146.8 ± 22.06***
UPG-107	224.8 ± 11.71	264.3 ± 20.71	320.8 ± 17.68***	315.6 ± 48.88	159.8 ± 7.3	248.2 ± 25.89**	541.8 ± 41.38***	263 ± 76.79	391.6 ± 38.83	121.9 ± 14.71***	373.5 ± 27.12	285 ± 40.73*
UPG-108	238.4 ± 9.53	336.6 ± 22.95**	507.7 ± 44.89***	245.7 ± 52.15	159.8 ± 7.39	265.4 ± 14.39***	215.7 ± 19.1*	164.2 ± 24.8	220.3 ± 17.48	218.8 ± 28	295.9 ± 15.6**	46.4 ± 2.7***
UPG-109	251.4 ± 15.43	208.6 ± 14.96	397 ± 51.12*	164 ± 36.54	159.8 ± 7.39	98.9 ± 5.9***	166.4 ± 26.41	119.5 ± 7.65**	220.3 ± 17.48	141.2 ± 19.52**	99.6 ± 7.54***	38.23 ± 7.85***
UPG-111	214.5 ± 10.51	179.2 ± 19.05	181.9 ± 9.5*	188.6 ± 15.77	152.4 ± 5.1	111.3 ± 6.17***	120.9 ± 8.6**	93.38 ± 9.41***	153.3 ± 10.75	251.5 ± 22**	148.9 ± 10.3	119.1 ± 17.68
UPG-112	279.9 ± 11.02	231.1 ± 24.14	386.5 ± 54.72*	126.2 ± 13.78***	242.6 ± 20.63	354.4 ± 28**	502.2 ± 39.15***	261.8 ± 27.3	323 ± 30.45	593 ± 24.94***	406.4 ± 40.28	457.6 ± 46.53

[a]The values of E_{max} (dyne/mg tissue) for ***h*U-II**, **U-II$^{(4-11)}$**, and **[Ala^1]U-II** are reported in the presence of peptides **UPG-106−109**, **UPG-111**, and **UPG-112** or vehicle in rat aorta (*$p < 0.05$; **$p < 0.001$; ***$p < 0.001$ vs own vehicle).

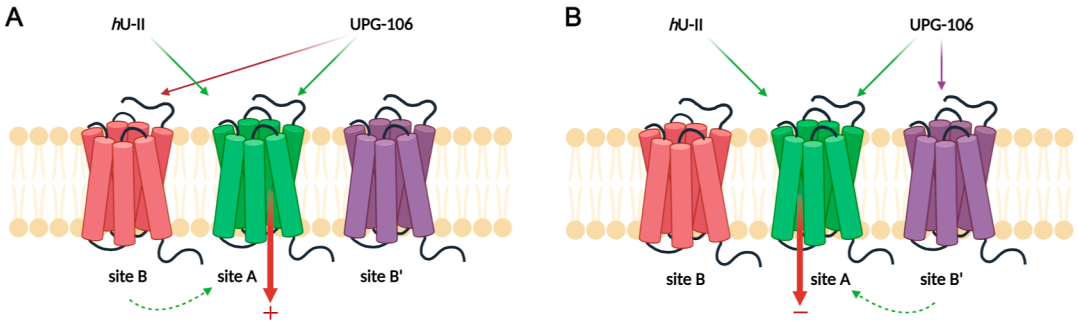

Figure 4. Multisites model of lateral allosteric modulation of the UTR receptor proposed for peptide **UPG-106** when tested at 0.1 and 1 μM concentration (A) or 10 μM (B), in competition with ***h*U-II** as probe compound. Binding sites are indicated as site-A (orthosteric site), site-B, and site-B' (allosteric sites).

discrepancy, these assays were selected to provide preliminary information on the behavior of our compounds. Regarding results from the calcium mobilization, it has been noted that **[Ala^1]U-II** elicited higher $[Ca^{2+}]_i$ than the parent ***h*U-II**, and **UPG-110** also showed an immediate activation of UTR already at 0.1 nM concentration. However, many analogues bearing the "antagonist" cyclic region, including **urantide** itself, were able to weakly increase the calcium concentration compared to the basal level. This effect was already reported for **urantide**,[47] indicating that in this assay, **urantide** can be preferentially considered a partial agonist. Interestingly, **urantide**-based derivatives, such as **UPG-106** and **UPG-108**, possessing Glu and Gln in position 1, respectively, showed high potency and efficiency to increase $[Ca^{2+}]_i$. **UPG-108** was able to elicit high $[Ca^{2+}]_i$ production, even at the lowest concentration used (0.1 nM), suggesting that switching from carboxylic acid to amide may result in increased potency. As above-described, discrepancies between the results of calcium mobilization and vasoconstriction assays for **urantide** and analogues may be attributed to species-specific differences between rat and human UT receptors, or to the different efficiency of stimulus-response coupling that characterizes the rat aorta and $[Ca^{2+}]_i$/(HEK-293)hUT assays, being low for the former and very high for the latter,[47] and/or to potentially different signaling pathways in the onset of the two effects raising the intriguing hypothesis that also these compounds can behave as biased modulators of UTR as already determined for urantide.[9]

Given that UTR ligands act as vasoconstricting agents, our peptides were further investigated to correlate intracellular calcium release with their contractile action. Outcomes gained by the contractile action in ex vivo rat aortic ring experiments indicated which derivatives had agonist activity. In this assay, peptides **UPG-106−109**, **UPG-111**, and **UPG-112**, carrying the "antagonist" cyclic sequence, [Pen-Phe-D-Trp-Orn-Tyr-Cys], were devoid of vasoconstriction activity, while only **UPG-110** and **UPG-113**, carrying the "agonist" cyclic sequence, [Cys-Phe-Trp-Lys-Tyr-Cys], were able to elicit a contractile response. Compared to the parent peptide ***h*U-II**, both peptides induced a contraction with lower efficacy, denoting that one single-point modification in the *N*-terminus is crucial for functional behavior, in agreement with literature data.[8,48] In fact, the importance of the electrostatic interaction between Glu^1 of *h*U-II and its receptor has been observed in previous docking studies.[8,48]

Peptides **UPG-106−109**, **UPG-111**, and **UPG-112**, all of which were unable to induce rat aortic ring contraction but some capable of activating internal signaling, were further investigated to explore their attitude to modulate the action of known UTR ligands. Therefore, in the rat aorta ring contraction competition assay, we considered probe agonists the endogenous ***h*U-II**, its analogue **U-II$^{(4-11)}$**, lacking the three N-terminal amino acids, and **[Ala^1]U-II**, possessing the mutation Glu^1/Ala^1. The last two probes, endowed with critical modifications concerning the N-terminus with respect to *h*U-II, a tripeptide truncation, and one key residue replacement,

https://doi.org/10.1021/acs.jmedchem.4c00688
J. Med. Chem. 2024, 67, 13879−13890

respectively, were selected to evaluate how their activity changes in the presence of a putative modulator bearing novel modifications in the same region. The competition assay led to numerous interesting and unexpected outcomes. Many compounds showed noncompetitive agonism/antagonism, which can be rationalized only by assuming the interaction with allosteric sites. The structural similarity of the developed analogues with the agonist probes strongly suggests that the allosteric sites are formed by receptor dimerization or, even, multimerization. Considering that UTR could exist as oligomers and the fact that these synthesized peptides, although sharing almost the same pharmacophore with *h*U-II, act noncompetitively, it is possible to advance the hypothesis that these allosteric modulators could influence the mediated pharmacological profile of *h*U-II through a phenomenon known as lateral allostery.[49,50] These compounds would be able to modulate the function of a receptor protomer by targeting another protomer of the complex. In this regard, a few studies have previously suggested the possible presence of UTR oligomers.[37,51] Following this hypothesis, we formulated a different mechanism of interaction between the reference agonists considered in this study, *h*U-II, U-II$^{(4-11)}$, and [**Ala**^{1}]U-II, which interact with the orthosteric site, and the peptides, which additionally may interact with allosteric site(s) (Figure 4). After the binding of the probe agonist to the orthosteric site (site-A), the tested compounds can interact with the same site-A inducing a competitive antagonism (decrease of the potency without affecting the efficacy and shifting of the concentration−response curve to the right). At the same time, tested compounds can interact with the allosteric sites (site-B and/or B′). The interaction with the allosteric sites can influence (i) the affinity of the probe with site-A, by increasing (higher affinity) or decreasing (lower affinity) the potency of the probe, (ii) the ability of the probe to stabilize a receptor conformation able to transmit a certain cytosolic signal (modulation of the efficacy), and (iii) the ability of the probe to induce receptor desensitization/internalization, decreasing the efficacy.

In light of this proposed model, the most interesting results from the rat aorta competition assays are herein discussed.

As for the impact on the UTR ligand efficacy, **UPG-106** increased the efficacy of *h*U-II at the lowest concentration (0.1 μM) and significantly at 1 μM, likely due to an allosteric interaction at site-B (Figure 4A), while a significant decrease in efficacy was observed at the highest concentration (10 μM) (Figure 4B). This fluctuating trend may depend on the specific conformational effect induced by **UPG-106** following its interaction with allosteric sites, as depicted in Figure 4. For instance, given that there are two allosteric sites (B and B′), which do not have affinity for the probe molecules, but for the tested ones, it can be assumed that at lower concentrations, **UPG-106** binds to an allosteric site (e.g., site-B), resulting in an increase of efficacy. At the highest concentration (10 μM), **UPG-106** also binds additional lower affinity allosteric sites (e.g., site-B′). Binding to both allosteric sites, B and B′, ultimately leads to a decrease in efficacy at this concentration, and **UPG-106** behaves as an insurmountable antagonist. Alternatively, when the number of occupied B sites exceeds a certain threshold, receptor desensitization/internalization occurs, leading to the observed decrease in efficacy. Therefore, the occupancy of allosteric sites, which depend on the concentration of the tested molecule, will determine the efficacy. The effects of **UPG-106** versus the other probes, U-II$^{(4-11)}$ and [**Ala**^{1}]U-II, are different. A probe-dependent effect is clearly observed as well as for other tested molecules. **UPG-107** has a notable positive effect on the efficacy of U-II$^{(4-11)}$, which may be due to allosteric interaction with the site-B. In contrast, **UPG-107** has negative effects on the efficacy versus [**Ala**^{1}]U-II. The effects induced by **UPG-108** in competition with the three agonist probes are very similar to each other, with a concentration-dependent increase in efficacy at the lowest or intermediate concentration. This outcome can be correlated to an allosteric effect: predominant binding to site-B at lower concentrations, effective binding at site-B′, or desensitization through site-B at the highest concentration. Noteworthy, *h*U-II achieves the maximum efficacy observed, approximately double its intrinsic efficacy, in the presence of 1 μM **UPG-108**. For **UPG-109**, *h*U-II efficacy decreased at 0.1 μM, increased at 1 μM, and decreased again at 10 μM, indicating site-B's positive role in efficacy at the intermediate concentration. Notably, considering the effect on [**Ala**^{1}]U-II, **UPG-109** reduced the efficacy in a concentration-dependent manner. Probably, when [**Ala**^{1}]U-II is bound to site-A, **UPG-109** cannot access site-B but only the negatively acting site-B'. **UPG-111** led to a decrease in efficacy at all concentrations except for [**Ala**^{1}]U-II at 0.1 μM. **UPG-112** showed fluctuating effects on the efficacy of *h*U-II, U-II$^{(4-11)}$ and [**Ala**^{1}]U-II, with an increase in efficacy for U-II$^{(4-11)}$ at 0.1 and 1 μM and for [**Ala**^{1}]U-II at 0.1 μM.

As for the impact on the potency of the UTR agonists, **UPG-106** decreased the potency of *h*U-II in a concentration-dependent manner that may result from either direct competition for site-A and/or an effect on *h*U-II affinity induced by an interaction of **UPG-106** with an allosteric site. Notably, the fluctuations observed for [**Ala**^{1}]U-II suggest that the allosteric binding of **UPG-106** also modulates the potency factor. **UPG-107** had a negative impact on the potency versus [**Ala**^{1}]U-II, which parallels the aforementioned reduction of efficacy. The fluctuating values of efficacy and potency at different concentrations of **UPG-107** can be assigned to the contrasting effects upon binding to the orthosteric (A) and allosteric (B, B′) sites. **UPG-108** showed a concentration-dependent decrease in potency when competing with the three agonist probes. **UPG-109** also induced a concentration-dependent decrease in the potency against the three probes. Interestingly, it behaves as a negative allosteric modulator (NAM) versus [**Ala**^{1}]U-II, reducing both efficacy and potency in a concentration-dependent manner. Taking into account also its negative effect on efficacy, **UPG-111** can be considered, at least against *h*U-II and U-II$^{(4-11)}$, a NAM. Notably, **UPG-112** displayed an increase in potency, albeit not significantly, at lower concentrations against U-II$^{(4-11)}$ and [**Ala**^{1}]U-II. Considering its positive effect on efficacy as well, **UPG-112** behaved as a positive allosteric modulator at the indicated concentrations against these two agonist probes.

On the basis of the proposed model (Figure 4), **urantide**, which acts as a surmountable antagonist versus *h*U-II up to 10 μM concentration[49] in the presence of *h*U-II, is able to bind site-A (or its binding to sites B and B′ has no effect). Clearly, the N-terminal tail of our tested urantide derivatives can deeply modify the ligand property. As a matter of fact, the **urantide** itself becomes an unsurmountable antagonist at the highest concentration (10 μM), when tested against **URP**.[49] Hence, in the presence of **URP**, at variance with *h*U-II, **urantide** can bind to an allosteric site of UTR exerting its uncompetitive action. Moreover, from the comparison of the effects on *h*U-II's

https://doi.org/10.1021/acs.jmedchem.4c00688
J. Med. Chem. 2024, 67, 13879−13890

contractile activity induced by our best performing *h*U-II NAM, **UPG-111**, and **urantide**,[50] it emerges that **UPG-111** has a capacity comparable to **urantide** in reducing the potency of *h*U-II and, most importantly, it showed the unprecedented ability to reduce the efficacy of *h*U-II pointing out to a potential overall improvement of the antagonist activity.

Other notable UTR ligands already reported in the literature, **urocontrin A** (UCA) and **[Pen^2,Pep^4]URP**,[44,49] are noncompetitive antagonists of *h*U-II. According to our model, they should bind site-B′ when *h*U-II is bound to site-A, exerting their negative allosteric action.

Similarly to the direct effect on the rat aorta contraction assay, there is not a clear correlation between the ability of the tested compounds to induce calcium release and their actions in aorta competition assays, probably resulting from the aforementioned dichotomy between the two assays. However, it can be observed that **UPG-109** and **UPG-111**, which were unable to induce calcium release (up to the concentration of 0.1 mM), behave as negative allosteric modulators at least on some probes, remarkably **UPG-111** on the endogenous UTR agonist *h*U-II. In parallel, **UPG-108**, which displayed an elevated ability to release calcium even at low concentrations, was able to increase the efficacy of *h*U-II at the maximum level that we could observe. These results suggest that the calcium release effect could be related to allosteric modulation. The relationship between calcium release and positive allosteric modulation involving some of the analogues will deserve further investigation.

Finally, it is clear that correlating the observed activity of developed peptides with their different chemical functionalities and therefore their interaction with the receptor is intricate for different reasons: (i) the N-terminal region of the peptides, where the mutated residue(s) is located, is very flexible as we have previously determined by NMR studies;[52] (ii) the N-terminal regions of *h*U-II and **urantide** establish interactions with extracellular loops of UTR, as we have determined in previous docking experiments,[8,53] also these loops are highly flexible compared to the transmembrane regions of the receptor; and (iii) for noncompetitive ligands, a multimeric receptor should be modeled in the absence of any experimental template.

In conclusion, we have developed novel UTR modulators that are able to influence the activity of *h*U-II and other UTR agonists used as probes. To explain the observed modulation of the efficacy/potency of these ligands, a multimeric UTR model was proposed, involving the concept of lateral allostery. Among the developed compounds, some showed an unprecedented ability to enhance the efficacy of *h*U-II. Among these, **UPG-108** induced the maximum observed efficacy of endogenous agonist *h*U-II, approximately double its intrinsic efficacy. Noteworthy, **UPG-109** and **UPG-111** act as NAM of UTR. Considering also their pseudoinability to elicit calcium release, **UPG-109** and **UPG-111** are promising *h*U-II antagonist compounds. In particular, **UPG-111** will merit further investigation as it could potentially overcome failures previously observed for **urantide**. Overall, our study will shed light on the complexity that a GPCR system can underlie and the growing potentials of its modulation.

EXPERIMENTAL SECTION

Materials and General Procedures. N^a-Fmoc-protected amino acids were used, such as Fmoc-Glu(O*t*Bu), Fmoc-Thr(*t*Bu), Fmoc-Pro, Fmoc-Asp(O*t*Bu), Fmoc-Cys(Trt), Fmoc-Phe, Fmoc-Trp(Boc), Fmoc-Lys(Boc), Fmoc-Tyr(*t*Bu), Fmoc-Val, Fmoc-Ala, and Fmoc-Gln(Trt), including unconventional ones such as Fmoc-Pen(Trt), Fmoc-DTrp(Boc), Fmoc-Orn(Boc), Fmoc-Dab(Boc), and Fmoc-*h*Ser(Trt), all were purchased from IRIS Biotech GmbH (Marktredwitz, Germany) or Fluorochem (Hadfield, United Kingdom). Activating and additive reagents such as *N*,*N*,*N*′,*N*′-tetramethyl-*O*-(1*H*-benzotriazol-1-yl) uranium hexafluorophosphate (HBTU), 1-hydroxybenzotriazole (HOBt), (1-cyano-2-ethoxy-2-oxoethylidenaminooxy)dimethylaminomorpholino-carbenium hexafluorophosphate (COMU), and ethylcyano-(hydroxyimino)acetate (Oxyma Pure) were commercially obtained from Merck Life Science (Milan, Italy). Also, Wang resin (0.96 mmol/g of loading substitution), *N*,*N*-diisopropylethylamine (DIEA), 4-(dimethylamino)pyridine (DMAP), acetic anhydride, and NCS were purchased from Merck Life Science (Milan, Italy). Piperidine and TFA were purchased from IRIS Biotech GmbH (Marktredwitz, Germany). Solvents for peptide synthesis, such as *N*,*N*-dimethylformamide (DMF), dichloromethane (DCM), diethyl ether (Et_2O), and for HPLC analyses and purifications, such as water, MeOH, and acetonitrile (MeCN), were of reagent grade acquired from commercial sources (Merck Life Science or VWR, Milan, Italy) and used without further purification.

Purification of peptides **UPG-106−113** was performed by RP-HPLC (Shimadzu Preparative Liquid Chromatograph LC-8A) equipped with a preparative column (Phenomenex Kinetex C18 column, 5 μm, 100 Å, 150 × 21.2 mm) using linear gradients of MeCN (0.1% TFA) in water (0.1% TFA), from 10 to 90% over 30 min, with a flow rate of 10 mL/min and UV detection at 220 nm. Final products were obtained by lyophilization of the appropriate fractions after removal of MeCN by rotary evaporation.

To determine purity of the peptides **UPG-106−113**, prior biological examination, analytical HPLC (Shimadzu Nexera Liquid Chromatograph LC-30AD) analyses were performed on a Phenomenex Kinetex reversed-phase column (C18, 5 μm, 100 Å, 150 × 4.6 mm) with a flow rate of 1 mL/min using a gradient of MeCN (0.1% TFA) in water (0.1% TFA), from 10 to 90% over 15 min, and UV detection at 220 nm, and confirmed purity was ≥95% (Figures S1−S8). The correct molecular ions were confirmed by an HRMS spectrometer (LTQ Orbitrap) (Figure S9).

Peptide Synthesis. Wang resin (0.2 mmol for each sequence; 0.96 mmol/g as loading, 100−200 mesh as particle size) was placed into a 10 mL plastic syringe tube equipped with Teflon filter, stopper, and stopcock, preswollen in DMF on an automated shaker at rt for 30 min, treated with Fmoc-Val-OH (4 equiv), HBTU (4 equiv), HOBt (4 equiv), DIEA (8 equiv), and a catalytic amount of DMAP (0.15 equiv), all suspended in DMF, and shaken for 3 h at rt. The resin was then washed with DMF (2 mL × 3) and DCM (2 mL × 3). To avoid potential parallel synthesis of side products, any remaining reactive resin sites were end-capped by treatment with acetic anhydride (2 equiv), DIEA (4 equiv), and DMAP (0.4 equiv) in DCM, and the resulting mixture was agitated for 16 h at rt. The resin was washed with DMF (2 mL × 3) and DCM (2 mL × 3). Sequences were then elongated by embracing the Fmoc-based ultrasound-assisted solid-phase method.[42] 20% piperidine in DMF solution was added to remove the Fmoc group, thus the tube reactor was placed in an ultrasonic bath (SONOREX RK 52 H by BANDELIN electronic, Germany) with the reaction mixture not exceeding the water level (0.5 + 1 min). After each step, filtering and DMF washings of the resin were executed (2 mL × 3). Couplings were performed by treatment with a solution of the Fmoc amino acid (2 equiv), COMU (2 equiv), Oxyma Pure (2 equiv), and DIEA (4 equiv) in DMF and exposing the resin to ultrasonic irradiation for 5 min. Upon construction of the target resin-bound linear peptides, resins were dried in vacuo and cleaved by treating with a cocktail of TFA/TIS/H_2O (95:2.5:2.5, v/v/v) for 3 h at rt. Peptides were recovered by precipitation with Et_2O and then centrifuged (6000 rpm for 15 min). The supernatants were carefully removed, and the resulting amorphous solids were dried. The formation of disulfide bridge between two cysteine residues was performed in solution phase and achieved by NCS oxidation protocol.[43] In particular, the crude

https://doi.org/10.1021/acs.jmedchem.4c00688
J. Med. Chem. 2024, 67, 13879−13890

peptide was dissolved in H_2O (0.5 mM), and NCS (1 equiv) solution in H_2O (5 mL) was added under stirring. The mixture was shaken for 15 min at rt and then lyophilized to yield crude peptides, which were purified by RP-HPLC to afford the respective peptide (**UPG-106−113**) as a white powder.

Peptide **UPG-106**—% purity ≥95%; t_R = 11.7 min [analytical HPLC, isocratic 10% MeCN (0.1% TFA) in H_2O (0.1% TFA) over 5 min, and gradient 10−90% MeCN (0.1% TFA) in H_2O (0.1% TFA) over 15 min, flow rate of 1 mL/min]; HRMS (ESI) *m/z*: calcd for molecular formula $C_{65}H_{88}N_{13}O_{18}S_2^+$ $[M + H]^+$, 1402.5806; found, 1402.5829 $[M + H]^+$ and 701.7939 $[(M+2H)/2]^+$.

Peptide **UPG-107**—% purity ≥95%; t_R = 11.7 min [analytical HPLC, isocratic 10% MeCN (0.1% TFA) in H_2O (0.1% TFA) over 5 min, and gradient 10−90% MeCN (0.1% TFA) in H_2O (0.1% TFA) over 15 min, flow rate of 1 mL/min]; HRMS (ESI) *m/z*: calcd for molecular formula $C_{63}H_{86}N_{13}O_{16}S_2^+$ $[M + H]^+$, 1344.5751; found, 1344.5754 $[M + H]^+$ and 672.7917 $[(M+2H)/2]^+$.

Peptide **UPG-108**—% purity ≥95%; t_R = 11.6 min [analytical HPLC, isocratic 10% MeCN (0.1% TFA) in H_2O (0.1% TFA) over 5 min, and gradient 10−90% MeCN (0.1% TFA) in H_2O (0.1% TFA) over 15 min, flow rate of 1 mL/min]; HRMS (ESI) *m/z*: calcd for molecular formula $C_{65}H_{89}N_{14}O_{17}S_2^+$ $[M + H]^+$, 1401.5966; found, 1401.6007 $[M + H]^+$ and 701.3027 $[(M+2H)/2]^+$.

Peptide **UPG-109**—% purity ≥95%; t_R = 11.3 min [analytical HPLC, isocratic 10% MeCN (0.1% TFA) in H_2O (0.1% TFA) over 5 min, and gradient 10−90% MeCN (0.1% TFA) in H_2O (0.1% TFA) over 15 min, flow rate of 1 mL/min]; HRMS (ESI) *m/z*: calcd for molecular formula $C_{64}H_{89}N_{14}O_{16}S_2^+$ $[M + H]^+$, 1373.6017; found, 1373.6089 $[M + H]^+$ and 687.3196 $[(M+2H)/2]^+$.

Peptide **UPG-111**—% purity ≥95%; t_R = 11.7 min [analytical HPLC, isocratic 10% MeCN (0.1% TFA) in H_2O (0.1% TFA) over 5 min, and gradient 10−90% MeCN (0.1% TFA) in H_2O (0.1% TFA) over 15 min, flow rate of 1 mL/min]; HRMS (ESI) *m/z*: calcd for molecular formula $C_{64}H_{88}N_{13}O_{17}S_2^+$ $[M + H]^+$, 1374.5857; found, 1374.5861 $[M + H]^+$ and 687.7972 $[(M+2H)/2]^+$.

Peptide **UPG-112**—% purity ≥95%; t_R = 11.9 min [analytical HPLC, isocratic 10% MeCN (0.1% TFA) in H_2O (0.1% TFA) over 5 min, and gradient 10−90% MeCN (0.1% TFA) in H_2O (0.1% TFA) over 15 min, flow rate of 1 mL/min]; HRMS (ESI) *m/z*: calcd for molecular formula $C_{62}H_{86}N_{13}O_{14}S_2^+$ $[M + H]^+$, 1300.5853; found, 1300.5858 $[M + H]^+$ and 650.7962 $[(M+2H)/2]^+$.

Peptide **UPG-110**—% purity ≥95%; t_R = 11.2 min [analytical HPLC, isocratic 10% MeCN (0.1% TFA) in H_2O (0.1% TFA) over 5 min, and gradient 10−90% MeCN (0.1% TFA) in H_2O (0.1% TFA) over 15 min, flow rate of 1 mL/min]; HRMS (ESI) *m/z*: calcd for molecular formula $C_{63}H_{87}N_{14}O_{16}S_2^+$ $[M + H]^+$, 1359.5860; found, 1359.5869 $[M + H]^+$ and 680.2968 $[(M+2H)/2]^+$.

Peptide **UPG-113**—% purity ≥95%; t_R = 11.5 min [analytical HPLC, isocratic 10% MeCN (0.1% TFA) in H_2O (0.1% TFA) over 5 min, and gradient 10−90% MeCN (0.1% TFA) in H_2O (0.1% TFA) over 15 min, flow rate of 1 mL/min]; HRMS (ESI) *m/z*: calcd for molecular formula $C_{63}H_{86}N_{13}O_{17}S_2^+$ $[M + H]^+$, 1360.5701; found, 1360.5730 $[M + H]^+$ and 680.7899 $[(M+2H)/2]^+$.

Cell Culture and Transfection. HEK-293 cells were grown in Dulbecco's modified Eagle's medium supplemented with 10% fetal bovine serum (both from Gibco, Life Technologies). HEK-293 cells were generally cultured in a 5% CO_2 atmosphere at 37 °C. The stably transfected HEK 293-UTR cell line was generated as previously described.[49]

Intracellular $[Ca^{2+}]_i$ Measurement on Single Cells. HEK-293 cells, plated on glass coverslips, were loaded with 10 μM Fura 2-AM for 30 min at 37 °C. At the end of the loading period, the coverslips were washed with normal Krebs solution (5.5 mM KCl, 160 mM NaCl, 1.2 mM $MgCl_2$, 1.5 mM $CaCl_2$, 10 mM glucose, and 10 mM HEPES-NaOH, pH 7.4) and then inserted in a perfusion chamber (Medical System) in which HEK-293 cells were perfused during $[Ca^{2+}]_i$ acquisition with the same solution containing each peptide at different concentrations. Fura-2AM experiments were carried out with a digital imaging system composed of an Axiovert200 microscope (Carl Zeiss) equipped with a FLUAR 40× oil objective lens, a MicroMax 512BFT cooled CCD camera (Princeton Instruments), a LAMBDA10−2 filter wheeler (Sutter Instruments), and MetaMorph/MetaFluor Imaging System software (Universal Imaging). Fluorescence intensity was measured every 3 s, illuminating cells alternatively at wavelengths of 340 and 380 nm. The emitted light was passed through a 512 nm barrier filter. Ratiometric values were automatically converted by the software to $[Ca^{2+}]_i$.[54] Each EC_{50} was obtained by fitting the data with the equation $a + b*\exp(-x/t)$, where "*a*" is the maximal response, "*b*" the basal response, "*x*" the drug concentration, and "*t*" represents the EC_{50}.

Animals. The experimental procedures conformed to the guidelines of the Italian and European Council law for animal care (EU Directive 2010/63/EU and DL 26/2014) were approved by the Animal Ethics Committee of the University of Naples Federico II and by the Italian Ministry of Health that comply with the ARRIVE guidelines.[55]

Organ Bath Bioassay. Male albino Wistar rats (250−270 g, Charles River, Calco, Italy) were housed in group cages under controlled temperature (23 ± 2 °C), humidity (range of 40−70%), and illumination (12 h light/dark cycles). Food and water were fed ad libitum. Rats were anesthetized with enflurane (5%) and euthanized in a CO_2 chamber (70%). The thoracic aorta was cleaned of surrounding tissue, and the endothelium was removed by gently rubbing the vessel intimal surface. The aorta was divided into 2−3 mm rings and then placed in a 3 mL organ bath filled with thermostated (37 °C) and oxygenated (95% O_2−5% CO_2) Krebs' solution (NaCl 118 mM, KCl 4.7 mM, $MgCl_2$ 1.2 mM, KH_2PO_4 1.2 mM, $CaCl_2$ 2.5 mM, $NaHCO_3$ 25 mM, and glucose 10.1 mM). The rings were connected to an isometric transducer (Fort 25, World Precision Instruments, 2Biological Instruments, Varese, Italy) associated with PowerLab 8/35 (World Precision Instruments, Biological Instruments, Varese, Italy). The rings were initially stretched until a resting tension of 0.5 g and then were allowed to equilibrate for at least 60 min. During this period, when necessary, the tension was adjusted to 0.5 g, and the bath solution was periodically changed.[56,57] In each set of experiments, rings were first challenged with phenylephrine (PE, 0.3 μM) until the responses were reproducible. To verify the absence of the endothelium, a cumulative concentration−response curve to acetylcholine (Ach, 10 nM to 3 μM) was performed in PE-precontracted rings.

To assess the agonist activity, cumulative concentration−response curves (1 nM−30 μM) were performed with the synthetic peptides under examination, i.e., **UPG-106**, **UPG-107**, **UPG-108**, **UPG-109**, **UPG-110**, **UPG-111**, **UPG-112**, and **UPG-113**. In another set of experiments, the antagonistic activity of each synthetic peptide was evaluated. Briefly, aortic rings were incubated for 30 min with different concentrations (0.1, 1, or 10 μM) of each synthetic peptide or vehicle, and thereafter a cumulative concentration−response curve of *h***U-II** (1 nM−30 μM), **U-II**$^{(4-11)}$ (1 nM−30 μM), or [**Ala**^{1}]**U-II** (1 nM−30 μM) was carried out. The contraction was expressed as dyne/mg tissue.

Statistical Analysis. Data are expressed as mean ± SEM. Statistical comparisons between controls and treated experimental groups were performed using the one-way ANOVA, followed by Newman Keul's test. $P < 0.05$ was considered statistically significant for calcium measurement.

Concentration−response curves were analyzed by sigmoidal nonlinear regression fit using the GraphPad Prism 8.0 program (San Diego, CA) to determine the molar concentration of the agonists producing 50% (EC_{50}) and the top value standard as maximal response (E_{max}) in the presence of each synthetic peptide tested or vehicle. EC_{50} and E_{max} were calculated as the mean ± SEM from 5 animals and expressed as μM or dyne/mg tissue, respectively. The results were analyzed by using one-sample *t*-test. A value of $p < 0.05$ was considered significant.

https://doi.org/10.1021/acs.jmedchem.4c00688
J. Med. Chem. 2024, 67, 13879−13890

■ ASSOCIATED CONTENT

Supporting Information

The Supporting Information is available free of charge at https://pubs.acs.org/doi/10.1021/acs.jmedchem.4c00688.

Analytical data of peptides **UPG106−113**; HPLC traces for the synthesized peptides; HRMS spectra of peptides **UPG106−113**; EC_{50} values for UTR ligands against **UPG106−109**, **UPG-111**, and **UPG-112** (PDF)

Molecular formula strings (CSV)

■ AUTHOR INFORMATION

Corresponding Authors

Francesco Merlino − *Department of Pharmacy, School of Medicine and Surgery, University of Naples Federico II, 80131 Naples, Italy; Centro Interuniversitario di Ricerca sui Peptidi Bioattivi "Carlo Pedone" (CIRPeB), University of Naples Federico II, 80134 Naples, Italy;* orcid.org/0000-0002-9607-229X; Email: francesco.merlino@unina.it

Paolo Grieco − *Department of Pharmacy, School of Medicine and Surgery, University of Naples Federico II, 80131 Naples, Italy; Centro Interuniversitario di Ricerca sui Peptidi Bioattivi "Carlo Pedone" (CIRPeB), University of Naples Federico II, 80134 Naples, Italy;* orcid.org/0000-0002-6854-8123; Email: paolo.grieco@unina.it

Authors

Agnese Secondo − *Division of Pharmacology, Department of Neuroscience, Reproductive and Dentistry Sciences, School of Medicine and Surgery, University of Naples Federico II, 80131 Naples, Italy*

Emma Mitidieri − *Department of Pharmacy, School of Medicine and Surgery, University of Naples Federico II, 80131 Naples, Italy*

Raffaella Sorrentino − *Department of Pharmacy, School of Medicine and Surgery, University of Naples Federico II, 80131 Naples, Italy*

Rosa Bellavita − *Department of Pharmacy, School of Medicine and Surgery, University of Naples Federico II, 80131 Naples, Italy;* orcid.org/0000-0003-2163-5163

Nicola Grasso − *Department of Pharmacy, School of Medicine and Surgery, University of Naples Federico II, 80131 Naples, Italy;* orcid.org/0000-0002-7961-7040

David Chatenet − *Institut National de la Recherche Scientifique (INRS), Centre Armand-Frappier Santé Biotechnologie, Université du Québec, H7 V 1B7 Québec, Canada*

Anna Pannaccione − *Division of Pharmacology, Department of Neuroscience, Reproductive and Dentistry Sciences, School of Medicine and Surgery, University of Naples Federico II, 80131 Naples, Italy*

Roberta d'Emmanuele di Villa Bianca − *Department of Pharmacy, School of Medicine and Surgery, University of Naples Federico II, 80131 Naples, Italy*

Alfonso Carotenuto − *Department of Pharmacy, School of Medicine and Surgery, University of Naples Federico II, 80131 Naples, Italy; Centro Interuniversitario di Ricerca sui Peptidi Bioattivi "Carlo Pedone" (CIRPeB), University of Naples Federico II, 80134 Naples, Italy;* orcid.org/0000-0001-7532-5449

Complete contact information is available at: https://pubs.acs.org/10.1021/acs.jmedchem.4c00688

Author Contributions

[⊥]R.d'E.d.V.B. and A.C. have equally shared the co-last authorship. The manuscript was written through the contributions of all authors. All authors have given approval to the final version of the manuscript.

Funding

This research work was supported by the grant from Regione Campania POR FERS 2014−2020—Project N. 61G18000470007.

Notes

The authors declare no competing financial interest.

■ ACKNOWLEDGMENTS

The authors are grateful to the personnel of the 'Laboratorio di Analisi Strumentale (LAS)', Department of Pharmacy, University of Naples Federico II, for the MS analyses.

■ ABBREVIATIONS

Dab, 2,4-diaminobutyric acid; *h*Ser, homoserine; *h*U-II, human urotensin II; U-II, urotensin II; URP, urotensin II related peptide; US-SPPS, ultrasonic-assisted solid-phase peptide synthesis; UTR, urotensin II receptor.

■ REFERENCES

(1) Nassour, H.; Iddir, M.; Chatenet, D. Towards targeting the urotensinergic system: overview and challenges. *Trends Pharmacol. Sci.* **2019**, *40*, 725−734.

(2) Vaudry, H.; Leprince, J.; Chatenet, D.; Fournier, A.; Lambert, D. G.; Le Mével, J. C.; Ohlstein, E. H.; Schwertani, A.; Tostivint, H.; Vaudry, D. International union of basic and clinical pharmacology. XCII. Urotensin II, Urotensin II−Related Peptide, and their receptor: from structure to function. *Pharmacol. Rev.* **2015**, *67*, 214−258.

(3) Chatenet, D.; Nguyen, T. T.; Létourneau, M.; Fournier, A. Update on the urotensinergic system: new trends in receptor localization, activation, and drug design. *Front. Endocrinol.* **2013**, *3*, 174.

(4) Pearson, D.; Shively, J. E.; Clark, B. R.; Geschwind, I. I.; Barkley, M.; Nishioka, R. S.; Bern, H. A. Urotensin II: a somatostatin-like peptide in the caudal neurosecretory system of fishes. *Proc. Natl. Acad. Sci. U.S.A.* **1980**, *77*, 5021−5024.

(5) Coulouarn, Y.; Lihrmann, I.; Jegou, S.; Anouar, Y.; Tostivint, H.; Beauvillain, J. C.; Conlon, J. M.; Bern, H. A.; Vaudry, H. Cloning of the cDNA encoding the urotensin II precursor in frog and human reveals intense expression of the urotensin II gene in motoneurons of the spinal cord. *Proc. Natl. Acad. Sci. U.S.A.* **1998**, *95*, 15803−15808.

(6) Leprince, J.; Chatenet, D.; Dubessy, C.; Fournier, A.; Pfeiffer, B.; Scalbert, E.; Renard, P.; Pacaud, P.; Oulyadi, H.; Ségalas-Milazzo, I.; Guilhaudis, L.; Davoust, D.; Tonon, M. C.; Vaudry, H. Structure-activity relationships of urotensin II and URP. *Peptides* **2008**, *29*, 658−673.

(7) Chatenet, D.; Dubessy, C.; Leprince, J.; Boularan, C.; Carlier, L.; Segalas-Milazzo, I.; Guilhaudis, L.; Oulyadi, H.; Davoust, D.; Scalbert, E.; Pfeiffer, B.; Renard, P.; Tonon, M. C.; Lihrmann, I.; Pacaud, P.; Vaudry, H. Structure-activity relationships and structural conformation of a novel urotensin II-related peptide. *Peptides* **2004**, *25*, 1819−1830.

(8) Brancaccio, D.; Merlino, F.; Limatola, A.; Yousif, A. M.; Gomez-Monterrey, I.; Campiglia, P.; Novellino, E.; Grieco, P.; Carotenuto, A. An investigation into the origin of the biased agonism associated with the urotensin II receptor activation. *J. Pept. Sci.* **2015**, *21*, 392−399.

(9) Brulé, C.; Perzo, N.; Joubert, J. E.; Sainsily, X.; Leduc, R.; Castel, H.; Prézeau, L. Biased signaling regulates the pleiotropic effects of the urotensin II receptor to modulate its cellular behaviors. *FASEB J.* **2014**, *28*, 5148−5162.

(10) Billard, E.; Iddir, M.; Nassour, H.; Lee-Gosselin, L.; Poujol de Molliens, M.; Chatenet, D. New directions for urotensin II receptor ligands. *Pept. Sci.* **2019**, *111*, No. e24056.
(11) Pereira-Castro, J.; Brás-Silva, C.; Fontes-Sousa, A. P. Novel insights into the role of urotensin II in cardiovascular disease. *Drug Discovery Today* **2019**, *24*, 2170−2180.
(12) Russell, F. D. Urotensin II in cardiovascular regulation. *Vasc. Health Risk Manage.* **2008**, *4*, 775−785.
(13) Ross, B.; McKendy, K.; Giaid, A. Role of urotensin II in health and disease. *Am. J. Physiol.: Regul., Integr. Comp. Physiol.* **2010**, *298*, R1156−R1172.
(14) Svistunov, A. A.; Tarasov, V. V.; Shakhmardanova, S. A.; Sologova, S. S.; Bagaturiya, E. T.; Chubarev, V. N.; Galenko-Yaroshevsky, P. A.; Avila-Rodriguez, M. F.; Barreto, G. E.; Aliev, G. Urotensin II: molecular mechanisms of biological activity. *Curr. Protein Pept. Sci.* **2018**, *19*, 924−934.
(15) Wang, Y.; Tian, W.; Xiu, C.; Yan, M.; Wang, S.; Mei, Y. Urantide improves the structure and function of right ventricle as determined by echocardiography in monocrotaline-induced pulmonary hypertension rat model. *Clin. Rheumatol.* **2019**, *38*, 29−35.
(16) Wang, T.; Xie, L.; Bi, H.; Li, Y.; Li, Y.; Zhao, J. Urantide alleviates the symptoms of atherosclerotic rats in vivo and in vitro models through the JAK2/STAT3 signaling pathway. *Eur. J. Pharmacol.* **2021**, *902*, 174037.
(17) Oh, K. S.; Lee, J. H.; Yi, K. Y.; Lim, C. J.; Park, B. K.; Seo, H. W.; Lee, B. H. A novel urotensin II receptor antagonist, KR-36996, improved cardiac function and attenuated cardiac hypertrophy in experimental heart failure. *Eur. J. Pharmacol.* **2017**, *799*, 94−102.
(18) Portnoy, A.; Kumar, S.; Behm, D. J.; Mahar, K. M.; Noble, R. B.; Throup, J. P.; Russ, S. F. Effects of Urotensin II receptor antagonist, GSK1440115, in asthma. *Front. Pharmacol* **2013**, *4*, 54.
(19) Castel, H.; Desrues, L.; Joubert, J. E.; Tonon, M. C.; Prézeau, L.; Chabbert, M.; Morin, F.; Gandolfo, P. The G protein-coupled receptor UT of the neuropeptide Urotensin II displays structural and functional chemokine features. *Front. Endocrinol.* **2017**, *8*, 76.
(20) Gravina, A. G.; Dallio, M.; Romeo, M.; Pellegrino, R.; Stiuso, P.; Lama, S.; Grieco, P.; Merlino, F.; Panarese, I.; Marino, F. Z.; Sangineto, M.; Romano, M.; Federico, A. The urotensin-II receptor: A marker for staging and steroid outcome prediction in ulcerative colitis. *Eur. J. Clin. Invest.* **2023**, *53*, No. e13972.
(21) Gravina, A. G.; Dallio, M.; Tuccillo, C.; Martorano, M.; Abenavoli, L.; Luzza, F.; Stiuso, P.; Lama, S.; Grieco, P.; Merlino, F.; Caraglia, M.; Loguercio, C.; Federico, A. Urotensin II receptor expression in patients with ulcerative colitis: a pilot study. *Minerva Gastroenterol. Dietol.* **2020**, *66*, 23−28.
(22) Suguro, T.; Watanabe, T.; Kodate, S.; Xu, G.; Hirano, T.; Adachi, M.; Miyazaki, A. Increased plasma urotensin-II levels are associated with diabetic retinopathy and carotid atherosclerosis in type 2 diabetes. *Clin. Sci.* **2008**, *115*, 327−334.
(23) Mitidieri, E.; di Villa Bianca, R.; Donnarumma, E.; Fusco, F.; Longo, N.; Rosa, G. D.; Novellino, E.; Grieco, P.; Mirone, V.; Cirino, G.; Sorrentino, R. A new therapeutic approach to erectile dysfunction: urotensin-II receptor high affinity agonist ligands. *Asian J. Androl.* **2015**, *17*, 81−85.
(24) d'Emmanuele di Villa Bianca, R.; Cirino, G.; Mitidieri, E.; Coletta, C.; Grassia, G.; Roviezzo, F.; Grieco, P.; Novellino, E.; Imbimbo, C.; Mirone, V.; Sorrentino, R. Urotensin II: a novel target in human corpus cavernosum. *J. Sex. Med.* **2010**, *7*, 1778−1786.
(25) Eyre, H. J.; Speight, T.; Glazier, J. D.; Smith, D. M.; Ashton, N. Urotensin II in the development and progression of chronic kidney disease following 5/6 nephrectomy in the rat. *Exp. Physiol.* **2019**, *104*, 421−433.
(26) Zappavigna, S.; Abate, M.; Cossu, A. M.; Lusa, S.; Campani, V.; Scotti, L.; Luce, A.; Yousif, A. M.; Merlino, F.; Grieco, P.; De Rosa, G.; Caraglia, M. Urotensin-II-targeted liposomes as a new drug delivery system towards prostate and colon cancer cells. *J. Oncol.* **2019**, *2019*, 9293560.
(27) Grieco, P.; Franco, R.; Bozzuto, G.; Toccacieli, L.; Sgambato, A.; Marra, M.; Zappavigna, S.; Migaldi, M.; Rossi, G.; Striano, S.; Marra, L.; Gallo, L.; Cittadini, A.; Botti, G.; Novellino, E.; Molinari, A.; Budillon, A.; Caraglia, M. Urotensin II receptor predicts the clinical outcome of prostate cancer patients and is involved in the regulation of motility of prostate adenocarcinoma cells. *J. Cell. Biochem.* **2011**, *112*, 341−353.
(28) Federico, A.; Zappavigna, S.; Dallio, M.; Misso, G.; Merlino, F.; Loguercio, C.; Novellino, E.; Grieco, P.; Caraglia, M. Urotensin-II receptor: a double identity receptor involved in vasoconstriction and in the development of digestive tract cancers and other tumors. *Curr. Cancer Drug Targets* **2017**, *17*, 109−121.
(29) Brkovic, A.; Hattenberger, A.; Kostenis, E.; Klabunde, T.; Flohr, S.; Kurz, M.; Bourgault, S.; Fournier, A. Functional and binding characterizations of urotensin II-related peptides in human and rat urotensin II-receptor assay. *J. Pharmacol. Exp. Ther.* **2003**, *306*, 1200−1209.
(30) Kinney, W. A.; Almond, H. R., Jr.; Qi, J.; Smith, C. E.; Santulli, R. J.; de Garavilla, L.; Andrade-Gordon, P.; Cho, D. S.; Everson, A. M.; Feinstein, M. A.; Leung, P. A.; Maryanoff, B. E. Structure-function analysis of urotensin II and its use in the construction of a ligand-receptor working model. *Angew. Chem., Int. Ed. Engl.* **2002**, *41*, 2940−2944.
(31) Merlino, F.; Di Maro, S.; Yousif, A. M.; Caraglia, M.; Grieco, P. Urotensin-II Ligands: An Overview from Peptide to Nonpeptide Structures. *J. Amino Acids* **2013**, *2013*, 979016.
(32) Carotenuto, A.; Auriemma, L.; Merlino, F.; Yousif, A. M.; Marasco, D.; Limatola, A.; Campiglia, P.; Gomez-Monterrey, I.; Santicioli, P.; Meini, S.; Maggi, C. A.; Novellino, E.; Grieco, P. Lead optimization of P5U and urantide: discovery of novel potent ligands at the urotensin-II receptor. *J. Med. Chem.* **2014**, *57*, 5965−5974.
(33) Patacchini, R.; Santicioli, P.; Giuliani, S.; Grieco, P.; Novellino, E.; Rovero, P.; Maggi, C. A. Urantide: an ultrapotent urotensin II antagonist peptide in the rat aorta. *Br. J. Pharmacol.* **2003**, *140*, 1155−1158.
(34) Pehlivan, Y.; Dokuyucu, R.; Demir, T.; Kaplan, D. S.; Koc, I.; Orkmez, M.; Turkbeyler, I. H.; Ceribasi, A. O.; Tutar, E.; Taysi, S.; Kisacik, B.; Onat, A. M. Palosuran treatment effective as bosentan in the treatment model of pulmonary arterial hypertension. *Inflammation* **2014**, *37*, 1280−1288.
(35) Trebicka, J.; Leifeld, L.; Hennenberg, M.; Biecker, E.; Eckhardt, A.; Fischer, N.; Pröbsting, A. S.; Clemens, C.; Lammert, F.; Sauerbruch, T.; Heller, J. Hemodynamic effects of urotensin II and its specific receptor antagonist palosuran in cirrhotic rats. *Hepatology* **2008**, *47*, 1264−1276.
(36) Behm, D. J.; McAtee, J. J.; Dodson, J. W.; Neeb, M. J.; Fries, H. E.; Evans, C. A.; Hernandez, R. R.; Hoffman, K. D.; Harrison, S. M.; Lai, J. M.; Wu, C.; Aiyar, N. V.; Ohlstein, E. H.; Douglas, S. A. Palosuran inhibits binding to primate UT receptors in cell membranes but demonstrates differential activity in intact cells and vascular tissues. *Br. J. Pharmacol.* **2008**, *155*, 374−386.
(37) Clozel, M.; Hess, P.; Qiu, C.; Ding, S. S.; Rey, M. The urotensin-II receptor antagonist palosuran improves pancreatic and renal function in diabetic rats. *J. Pharmacol. Exp. Ther.* **2006**, *316*, 1115−1121.
(38) Merlino, F.; Billard, E.; Yousif, A. M.; Di Maro, S.; Brancaccio, D.; Abate, L.; Carotenuto, A.; Bellavita, R.; d'Emmanuele di Villa Bianca, R.; Santicioli, P.; Marinelli, L.; Novellino, E.; Hebert, T. E.; Lubell, W. D.; Chatenet, D.; Grieco, P. Functional selectivity revealed by N-methylation scanning of human Urotensin II and related peptides. *J. Med. Chem.* **2019**, *62*, 1455−1467.
(39) Billard, E.; Hebert, T. E.; Chatenet, D. Discovery of new allosteric modulators of the urotensinergic system through substitution of the Urotensin II-Related Peptide (URP) phenylalanine residue. *J. Med. Chem.* **2018**, *61*, 8707−8716.
(40) Merlino, F.; Yousif, A. M.; Billard, E.; Dufour-Gallant, J.; Turcotte, S.; Grieco, P.; Chatenet, D.; Lubell, W. D. Urotensin II$^{(4-11)}$ azasulfuryl peptides: synthesis and biological activity. *J. Med. Chem.* **2016**, *59*, 4740−4752.

https://doi.org/10.1021/acs.jmedchem.4c00688
J. Med. Chem. 2024, 67, 13879−13890

(41) Chatenet, D.; Nguyen, Q. T.; Letourneau, M.; Dupuis, J.; Fournier, A. Urocontrin, a novel UT receptor ligand with a unique pharmacological profile. *Biochem. Pharmacol.* **2012**, *83*, 608−615.
(42) Merlino, F.; Tomassi, S.; Yousif, A. M.; Messere, A.; Marinelli, L.; Grieco, P.; Novellino, E.; Cosconati, S.; Di Maro, S. Boosting Fmoc solid-phase peptide synthesis by ultrasonication. *Org. Lett.* **2019**, *21*, 6378−6382.
(43) Postma, T. M.; Albericio, F. N-chlorosuccinimide, an efficient reagent for on-resin disulfide formation in solid-phase peptide synthesis. *Org. Lett.* **2013**, *15*, 616−619.
(44) Chatenet, D.; Letourneau, M.; Nguyen, Q. T.; Doan, N. D.; Dupuis, J.; Fournier, A. Discovery of new antagonists aimed at discriminating UII and URP-mediated biological activities: insight into UII and URP receptor activation. *Br. J. Pharmacol.* **2013**, *168*, 807−821.
(45) Onan, D.; Hannan, R. D.; Thomas, W. G. Urotensin II: the old kid in town. *Trends Endocrinol. Metab.* **2004**, *15*, 175−182.
(46) Douglas, S. A.; Dhanak, D.; Johns, D. G. From 'gills to pills': urotensin-II as a regulator of mammalian cardiorenal function. *Trends Pharmacol. Sci.* **2004**, *25*, 76−85.
(47) Camarda, V.; Song, W.; Marzola, E.; Spagnol, M.; Guerrini, R.; Salvadori, S.; Regoli, D.; Thompson, J. P.; Rowbotham, D. J.; Behm, D. J.; Douglas, S. A.; Calo', G.; Lambert, D. G. Urantide mimics urotensin-II induced calcium release in cells expressing recombinant UT receptors. *Eur. J. Pharmacol.* **2004**, *498*, 83−86.
(48) Lescot, E.; Sopkova-de Oliveira Santos, J.; Colloc'h, N.; Rodrigo, J.; Milazzo-Segalas, I.; Bureau, R.; Rault, S. Three-dimensional model of the human urotensin-II receptor: docking of human urotensin-II and nonpeptide antagonists in the binding site and comparison with an antagonist pharmacophore model. *Proteins* **2008**, *73*, 173−184.
(49) Billard, E.; Chatenet, D. Insights into the molecular determinants involved in Urocontrin and Urocontrin A action. *ACS Med. Chem. Lett.* **2020**, *11*, 1717−1722.
(50) Billard, E.; Hébert, T. E.; Chatenet, D. Exploration of the urocontrin A scaffold yields new urotensinergic system allosteric modulator and competitive antagonists. *Biochem. Pharmacol.* **2023**, *211*, 115485.
(51) Castel, H.; Diallo, M.; Chatenet, D.; Leprince, J.; Desrues, L.; Schouft, M. T.; Fontaine, M.; Dubessy, C.; Lihrmann, I.; Scalbert, E.; Malagon, M.; Vaudry, H.; Tonon, M. C.; Gandolfo, P. Biochemical and functional characterization of high-affinity urotensin II receptors in rat cortical astrocytes. *J. Neurochem.* **2006**, *99*, 582−595.
(52) Grieco, P.; Carotenuto, A.; Patacchini, R.; Maggi, C. A.; Novellino, E.; Rovero, P. Design, synthesis, conformational analysis, and biological studies of urotensin-II lactam analogues. *Bioorg. Med. Chem.* **2002**, *10*, 3731−3739.
(53) Merlino, F.; Brancaccio, D.; Yousif, A. M.; Piras, L.; Campiglia, P.; Gomez-Monterrey, I.; Santicioli, P.; Meini, S.; Maggi, C. A.; Novellino, E.; Carotenuto, A.; Grieco, P. Structure-activity study of the peptides P5U and Urantide by the development of analogues containing uncoded amino acids at position 9. *ChemMedChem* **2016**, *11*, 1856−1864.
(54) Grynkiewicz, G.; Poenie, M.; Tsien, R. Y. A new generation of Ca2+ indicators with greatly improved fluorescence properties. *J. Biol. Chem.* **1985**, *260*, 3440−3450.
(55) Percie du Sert, N.; Hurst, V.; Ahluwalia, A.; Alam, S.; Avey, M. T.; Baker, M.; Browne, W. J.; Clark, A.; Cuthill, I. C.; Dirnagl, U.; Emerson, M.; Garner, P.; Holgate, S. T.; Howells, D. W.; Karp, N. A.; Lazic, S. E.; Lidster, K.; MacCallum, C. J.; Macleod, M.; Pearl, E. J.; Petersen, O. H.; Rawle, F.; Reynolds, P.; Rooney, K.; Sena, E. S.; Silberberg, S. D.; Steckler, T.; Würbel, H. The ARRIVE guidelines 2.0: updated guidelines for reporting animal research. *PLoS Biol.* **2020**, *18*, 3000410.
(56) Grieco, P.; Carotenuto, A.; Campiglia, P.; Gomez-Monterrey, I.; Auriemma, L.; Sala, M.; Marcozzi, C.; d'Emmanuele di Villa Bianca, R.; Brancaccio, D.; Rovero, P.; Santicioli, P.; Meini, S.; Maggi, C. A.; Novellino, E. New insight into the binding mode of peptide ligands at Urotensin-II receptor: structure-activity relationships study on P5U and urantide. *J. Med. Chem.* **2009**, *52*, 3927−3940.
(57) di Villa Bianca, R. d.; Sorrentino, R.; Mitidieri, E.; Marzocco, S.; Autore, G.; Thiemermann, C.; Pinto, A.; Sorrentino, R. Recombinant human erythropoietin prevents lipopolysaccharide-induced vascular hyporeactivity in the rat. *Shock* **2009**, *31*, 529−534.

https://doi.org/10.1021/acs.jmedchem.4c00688
J. Med. Chem. 2024, 67, 13879−13890